Journal of Catalysis 258 (2008) 366–377

Contents lists available at ScienceDirect

Journal of Catalysis

www.elsevier.com/locate/jcat

Effect of Pt and Pd promoter on Ni supported catalysts—A TPR/TPO/TPD and microcalorimetry study

A. Tanksale [a], J.N. Beltramini [a,*], J.A. Dumesic [b], G.Q. Lu [a]

[a] ARC Centre of Excellence for Functional Nanomaterials, University of Queensland, Brisbane, Queensland 4072, Australia
[b] Chemical and Biological Engineering Department, University of Wisconsin, Madison, WI 53706, USA

ARTICLE INFO

Article history:
Received 2 May 2008
Revised 12 June 2008
Accepted 20 June 2008
Available online 21 July 2008

Keywords:
Bimetallic catalysts
TPR
TPD
Microcalorimetry
Sorbitol reforming

ABSTRACT

The promoting effect of Pt and Pd in bimetallic Ni–Pt and Ni–Pd catalysts supported on alumina nanofibre (Alnf) were tested for the liquid phase reforming of sorbitol to produce hydrogen. The mono- and bimetallic catalysts were studied by different characterisation techniques such as: temperature programmed reduction, oxidation, CO desorption, microcalorimetry, TEM and STEM/EDX. Although bimetallic catalysts have long been the subject of great interest because of their exceptional properties compared to the monometallic catalysts, the reason behind their improved activity is still a question of debate. Experimental evidence showed that the addition of both Pt and Pd—even in a very small fraction—to the Ni catalyst increases its reducibility significantly. The TEM and STEM/EDX analysis confirmed that Pt and Ni are present as alloys in nano-sized rod shaped particles. At the same time it was found that the CO differential heat of adsorption is appreciably lowered in the bimetallic catalysts. This is substantial because reducing the CO binding strength can avoid the poisoning of the active metal sites. As a result, we demonstrate that the rate of H_2 formation from sorbitol reforming was 3 to 5 times higher for bimetallic catalysts when compared to the monometallic catalysts.

1. Introduction

Due to rising fuel prices, efforts to improve catalysts for production of alternative fuels have increased in the last few years. Hydrogen production from biomass is one of the most prevailing research areas in this regard. Hydrogen is considered one of the best alternative fuels because of its environmental benefits and high efficiency for energy production in fuel cells. However, hydrogen as a fuel will be able to reduce greenhouse gas emissions only when the source of hydrogen is environmentally benign such as water or biomass. But since water electrolysis is an energy-intensive process it requires a cheap and renewal source of electricity for it to be efficient. Currently photovoltaic cells, however, are not a viable energy source for water electrolysis. The focus is thus on biomass, which is cheap and abundant. Its high water content makes it unsuitable for gasification or steam reforming, but reforming of the biomass in the liquid phase is possible. After the introduction of aqueous phase reforming of alcohols and ethylene glycol [1–3], further studies [4] suggested that hydrogen can be directly produced from aqueous solutions of sugar or sugar alcohols.

From our previous studies [5] and the literature [6–8] we observed that the activity of the catalyst can be greatly enhanced using a bimetallic catalyst. It has also been suggested that the addition of noble metals to a Ni catalyst may reduce coke deposition and therefore provide stability [9]. The Ni–Pt system in particular has been extensively studied because of its synergetic catalytic effect [10–13]. Reducibility and kinetic studies for various reactions on Ni–Pt system supported on silica and alumina have also been reported [10,11,14–16]. Ko et al. [17] conducted CO chemisorption on mono- and bimetallic catalysts of Ni and Pt supported on γ-Al_2O_3 to study preferential oxidation (PROX) of CO in hydrogen rich stream. Their study showed that under the same pre-treatment condition Ni–Pt bimetallic catalysts had higher number of active sites. Moreover, the activity and selectivity of the bimetallic catalyst per unit site of the catalyst was also found to be higher for the PROX reaction. However, the reason for this was not clear beyond the enhanced reducibility of bimetallic catalysts. One of the reasons could be that the catalyst was more resistant to oxidation under the reaction condition [25]. It may also be possible that CO adsorption is altered on bimetallic catalysts due to surface heterogeneity creating favourable reaction conditions. Several probe molecules and surface reactions have been conducted to study adsorption behaviour of bimetallic catalysts [18–20]. However, the effect of noble metals on the CO chemisorption properties of the bimetallic supported catalysts has been less understood. In this study we aim to correlate the effect of the noble metal promoters such as Pt and Pd on Ni, using temperature programmed reduction (TPR), oxidation (TPO) and CO desorption (TPD). Heat-

* Corresponding author. Fax: +61 7 3346 3973.
E-mail address: jorgeb@uq.edu.au (J.N. Beltramini).

0021-9517/$ – see front matter
doi:10.1016/j.jcat.2008.06.024

flow microcalorimetry was employed to determine the strength of CO interaction on these catalysts. CO interaction with the catalyst is of high importance because a strong interaction can lead to catalyst poisoning [21]. It has been suggested that weaker interaction can decrease the heat of adsorption of CO and hydrogen chemisorption, thereby increasing the fraction of the surface available for the reforming reaction [22]. Reducing the amount of precious noble metal content also reduces the cost of the catalysts.

2. Experiments and methods

2.1. Catalyst preparation

The catalysts used in this study were prepared using the wet impregnation technique. Hydrogen hexacholoroplatinate(IV) (8% solution in water, Aldrich) was used as a precursor for the platinum catalyst, while nickel nitrate ($Ni(NO_3)_2{\cdot}6H_2O$, Univar) as a source of nickel and palladium(II) nitrate solution (10 wt% $Pd(NO_3)_2$ solution in 10 wt% nitric acid, Aldrich) for palladium catalysts. The impregnated Pt, Pd and Ni catalysts were prepared by adding appropriate amounts of solution of precursor to the support with constant stirring at 60 °C for 6 h. The catalysts were then dried overnight at 90 °C followed by calcination at 500 °C. Pt, Pd and Ni were supported on high surface area alumina nano-fibre (Alnf). For alumina nano-fibre preparation, glycerol was mixed with an appropriate amount of acid solution of $AlCl_3{\cdot}6H_2O$ and then a basic solution of $NaAlO_2$ was added drop-wise. The final pH of the solution was maintained at 6. The precipitate was collected by centrifugation. The precipitate was then washed several times to remove Na^+ and Cl^- ions. The washed cake was then mixed with PEO surfactant Tergitol 15TS-7. After prolonged stirring and ageing at 100 °C the resultant supernatant liquid was thrown and the white cake was dried in air and calcined at 500 °C for 20 h.

2.2. Characterisation of catalyst

Alumina nano-fibre surface area was measured using the BET technique employing nitrogen physisorption at the temperature of liquid nitrogen in a Quantachrome Autosorb-1C instrument. The percentage of metal loading was measured by Inductively-Coupled Plasma Atomic Emission Spectrometer (ICPAES).

2.2.1. TPR/TPO/TPD

Temperature programmed characterisation, such as reduction (TPR), oxidation (TPO) and desorption (TPD), was carried out using a setup illustrated in Fig. 1. Probe gases, attached to Brooks 5850E mass flow controllers of suitable flow range, were passed through a quartz glass reactor in a tube furnace. The gases were continuously sampled downstream through a 25 μm capillary connected to a Varian leak valve. The leak valve introduced gases in a vacuum chamber attached to SRS RGA300 quadrupole mass spectrometer. Varian MiniTask, with a maximum pumping speed of 40 L/s (for nitrogen) and base pressure of 1.5×10^{-7} Torr, was used to evacuate the vacuum chamber. The partial pressures of the gases evolved from the sample were recorded with respect to time, which was then converted to temperature according to the ramp rate of the furnace. Partial pressures were then converted to μmol/min using the calibration from standard gas mixtures at a measured flow rate in ml/min. TPR was conducted with 5% H_2/N_2 mixed gas at a flow rate of 50 ml/min. TPO was conducted with 2% O_2/He mixed gas at a flow rate of 50 ml/min. In both cases the temperature was raised from room temperature to 700 °C at the rate of 10 °C/min. For CO–TPD catalysts were pre-reduced in situ at 500 °C for Ni catalysts and 300 °C for Pt and Pd catalysts using ultrapure H_2 at a flow rate of 80 ml/min for 5 h. The catalysts were then purged with He at 100 ml/min flow rate, at the reduction temperature for 1 h. The catalysts were cooled to room temperature and dosed with CO at 100 ml/min for 15 min. The whole system, including the catalyst, was then flushed with He at 100 ml/min for at least 1 h to remove any trace of CO. For TPD measurements the temperature was raised from room temperature to 700 °C at the rate of 10 °C/min.

2.2.2. Microcalorimetry

Microcalorimetry measurements were performed at 30 °C using a Setaram BT2.15 heat-flux calorimeter. The calorimeter was connected to a high vacuum gas-handling and volumetric system employing Baratron capacitance manometers for precision pressure measurement of $\pm 0.5 \times 10^{-4}$ Torr. The maximum apparent leak

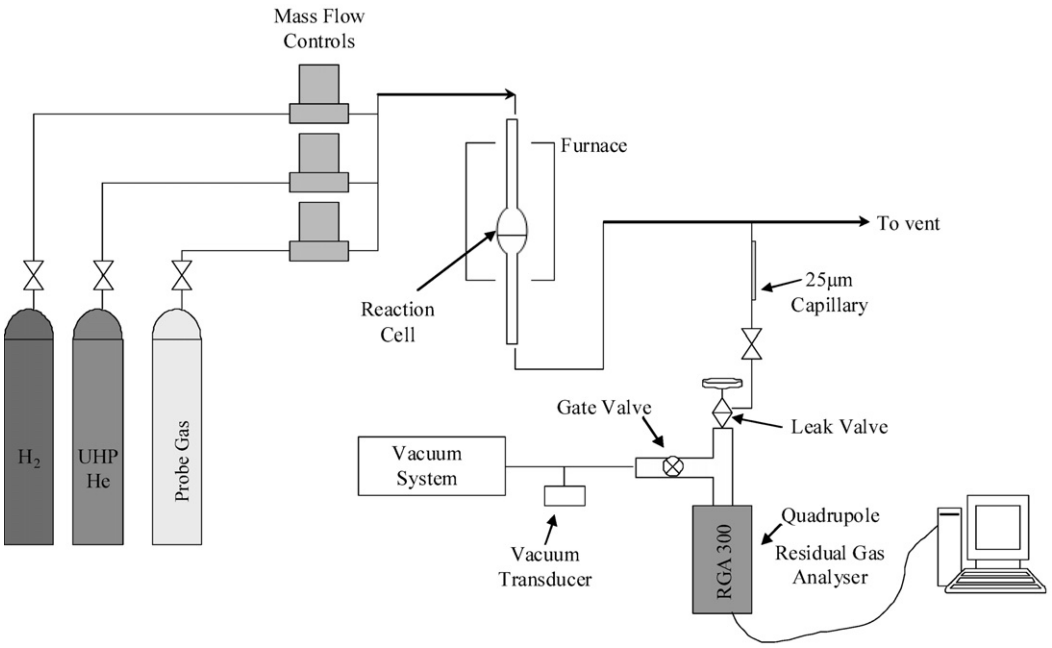

Fig. 1. Setup for temperature programmed characterisation.

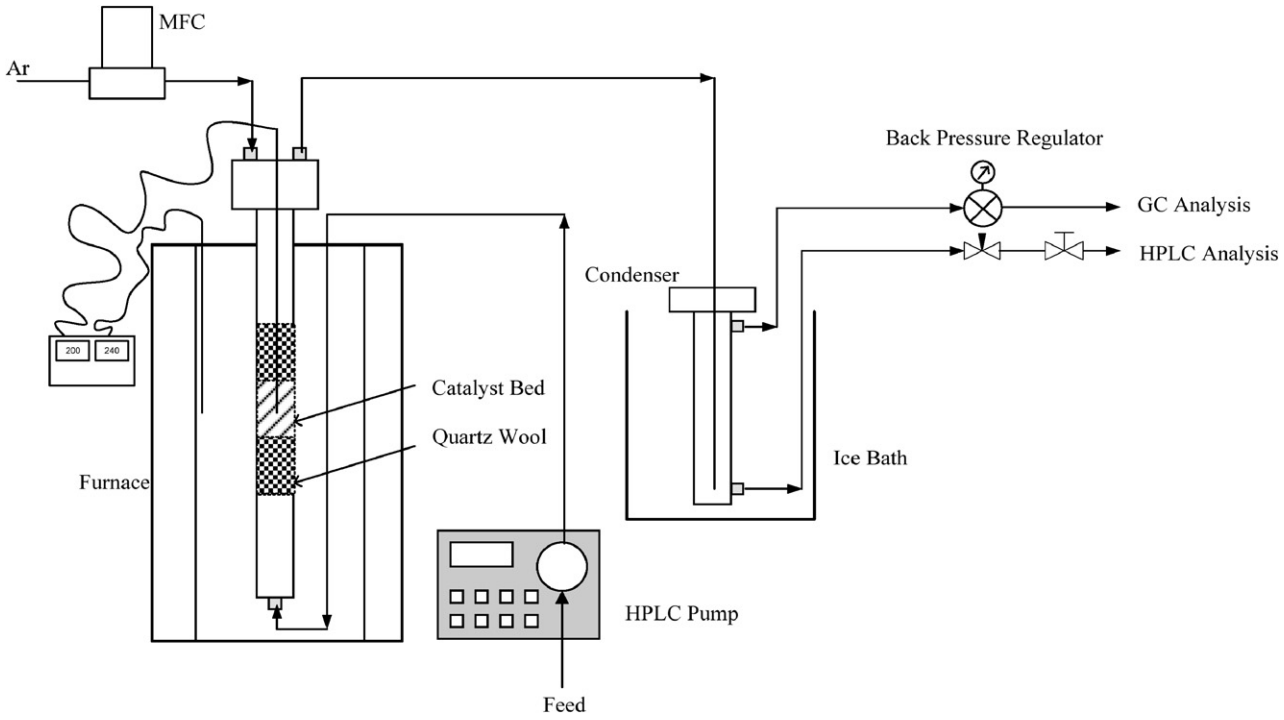

Fig. 2. Reaction kinetics setup for liquid phase reforming.

rate of the volumetric system, including the calorimetric cells, was in the range of 10^{-6} Torr/min. The ultimate dynamic vacuum of the system was 10^{-7} Torr. The calorimetric procedures used in this study have been described in detail elsewhere [23]. Briefly, each catalyst sample was reduced ex situ in ultrapure flowing H_2, followed by purging in ultrahigh purity He and sealing the sample in a Pyrex capsule at ca. 350 Torr. The Pyrex capsule containing the sample was then broken in a special set of calorimetric cells [24] after the sample had attained thermal equilibrium with the calorimeter. After the capsule had been broken the He pressure in the cell was reduced to ca. 1 Torr. The microcalorimetry data were collected by sequentially introducing small doses of CO (1–5 μmol) onto the catalyst (0.2–0.3 g) until it became saturated. The resulting heat response for each dose was recorded as a function of time and integrated to determine the energy released (mJ). The amount of gas adsorbed (μmol) was determined volumetrically from the dose and equilibrium pressures and the system volumes and temperatures. The differential heat (kJ/mol), defined as the negative of the enthalpy change of adsorption per mole of gas adsorbed, was then calculated as a function of the adsorbate coverage.

The CO-chemisorption experiments were conducted in the same vacuum gas-handling and volumetric system described above. The catalysts were reduced in situ in a Pyrex cell in flowing ultrahigh purity H_2 followed by purging with ultrahigh purity He and evacuation for 60 min at reduction temperature. Adsorption isotherm data was collected by sequentially introducing small doses of CO onto the catalyst until it became saturated. The cell was then evacuated for at least 1 h before second isotherm data was collected by introducing similar doses.

2.2.3. TEM and STEM/EDS Study

The calcined catalysts were suspended on a 3 mm holey carbon support film on a copper grid and were analysed in a Philips Tecnai 20 and a JEOL 2010 transmission electron microscope (TEM). The analytical resolution of Tecnai 20 is a result of the high brightness field emission gun (FEG), which acts as the electron source in this microscope. EDAX thin-window energy dispersive X-ray spectrometer (EDX) was used on the Techai 20 in scanning tunnelling electron microscope (STEM) mode.

2.3. Reaction kinetic study

The liquid phase reforming reactions were carried out in a fixed bed reactor (Fig. 2) at 200 °C and 20 bar pressure. Prior to starting the reforming reaction the catalysts were reduced in situ with high purity H_2 for at least 5 h at an appropriate reduction temperature followed by 15 min purging with Ar. The temperature of the reactor and furnace were controlled by individual PID controllers, which were placed in series such that the temperature over-limit inside the reactor would limit the current supply to the furnace controller. Both furnace and reactor temperatures were measured by OneTemp K-type thermocouples. A Swagelok back pressure regulator attached to a Swagelok pressure gauge was used to pressurise the system and a Brooks 5850E mass flow controller was employed for precise flow of Ar. 10% (w/w) concentration of sorbitol in water was fed in to the fixed bed reactor at a weight hourly space velocity of 6.2 h^{-1} (defined as feed mass flow rate in gm h^{-1}/mass of catalyst bed in gm).

Gas samples were analysed at 1 h intervals in a Shimadzu GC17A gas chromatographer employing 80/100 mesh carbosphere 1/8" I.D., 6 ft long packed column. Thermal conductivity and flame ionisation detectors were used to analyse H_2 and carbon compounds respectively. Sorbitol solutions were analysed in an HPLC using an external source to calculate the concentration of spent liquor. Shimadzu GCMS-QP5050A was used to qualitatively analyse the spent liquor for other organic compounds. The solid phase microextraction (SPME) technique was used to extract the organic compounds by heating the spent liquor to 95 °C in a glass vial with Teflon septa cap. 100 μm polydimethylsiloxane (PDMS) Supleco SPME fibre was used to adsorb the vapours of the organic compounds.

Table 1
Surface properties of the catalysts

Catalyst	Metal loading (% w/w)[a]		CO uptake (μmol/gm)	Reversible CO uptake (μmol/gm)	Metal surface area (m^2/gm Cat)	Dispersion (%)	BET surface area[b] (m^2/gm)
Pt/Alnf	2.905	(3)	111.61	16.81	4.89	53.60	360.47
Ni/Alnf	10.155	(10)	90.16	15.36	2.37	3.56	
Pd/Alnf	2.953	(3)	76.80	10.95	2.84	18.60	
Ni–Pt/Alnf	Ni—9.071	(10)	120.81	24.91	2.92	4.62	
	Pt—0.997	(1)					
Ni–Pd/Alnf	Ni—9.523	(10)	93.05	22.33	2.07	2.95	
	Pd—0.981	(1)					

[a] The values of metal loading given were measured by the ICPAES analysis; the values in parenthesis are the nominal values.
[b] The BET surface area is given for the calcined alumina nano-fibre support. It is expected that after impregnation the surface area of the catalysts will reduce slightly.

3. Results and discussion

3.1. CO-chemisorption

Table 1 shows the results of metal loading, support BET surface area and CO-chemisorption analysis. For CO-chemisorption analysis two isotherms were generated, first corresponding to the combined strong and weak adsorption and the second corresponding to only weak adsorption. Both the isotherms were Langmuir Type 1, characteristic of monolayer chemisorption, with the former corresponding mostly to fast strong adsorption on metal sites and the latter corresponding to slow weak adsorption on the metal oxide support. The CO-uptake (μmol/gm) in Table 1 is the total CO uptake i.e. weak and strong adsorption combined. However, the metal surface area and dispersion is calculated on the basis of monolayer adsorption of CO on the metal sites only. Therefore, only strong CO adsorption is considered for these calculations. The metal surface area and dispersion was calculated according to the following equations

$$\mathrm{SA}_m\ (\mathrm{m}^2/\mathrm{gm}-\mathrm{Cat}) = M_{\mathrm{CO}} \times \mathrm{SF} \times \mathrm{N} \times \mathrm{A}, \tag{1}$$

$$D\ (\%) = \frac{M_{\mathrm{CO}} \times \mathrm{SF} \times \mathrm{FW}_m}{\mathrm{WF}_m} \times 100, \tag{2}$$

where, M_{CO} is the monolayer CO adsorption in μmol/gm, SF is the stoichiometric factor i.e. metal:CO ratio in chemisorption, which was taken as 1 [25], $N = 6.023 \times 10^{23}$ is the Avogadro's number, A is the atomic cross section of the metal which was taken as 0.0649 nm^2 for Ni, 0.0984 nm^2 for Pt and 0.0897 nm^2 for Pd, FW_m is the formula weight of the metal and WF_m is the weight fraction of the metal in the catalyst. For bimetallic catalysts the metal surface area and dispersion were calculated assuming that the surface concentration of the metals was equal to bulk concentration [10].

The chemisorption results suggest that the addition of both Pt and Pd to Ni catalyst increases the number of active metal sites (measured as the total CO-uptake). We also observed an increase in specific metal surface area and dispersion for Ni–Pt bimetallic catalysts. This can be simply explained by the high formula weight and therefore high number of atoms per mol of Pt and Pd. In addition, the NiO particles are catalysed by Pt and Pd during the reduction process and therefore the number of Ni particles available for adsorption is greatly enhanced [10].

3.2. Temperature programmed reduction results

The results of CO-chemisorption can be supported by the TPR result shown in Fig. 3a. Ni/Alnf was tested for reducibility up to 820 °C and it exhibited two peaks at 700 and 800 °C. These high temperature peaks can be associated with the reduction peak of NiO which is in strong interaction with alumina support. It is known from literature [26] that calcination has a strong impact on the reducibility of Ni catalysts. In this study all the catalysts were calcined at 500 °C and the reduction peaks of Ni/Alnf is in close agreement with the results published by Rynkoswski et al. [26] at similar calcination temperature. The addition of Pt and Pd decreases the reduction peak of Ni–Pt/Alnf and Ni–Pd/Alnf to 450 and 550 °C respectively. Two shoulder peaks can be found either side of the maximum peak for both the bimetallic catalysts. The shoulder peak at higher temperature corresponds to the second Ni reduction peak observed for monometallic Ni/Alnf but, in this case, it is closer to the first reduction peak. The shoulder peak for Ni–Pt/Alnf at 265 °C is likely to be the Ni–Pt alloy reduction peak because it is at a higher temperature than the Pt/Alnf reduction peak (215 °C), suggesting that Pt particles are in close vicinity to the Ni particles. Therefore, due to the non-uniform nature of the catalyst surface, Pt can catalyse the NiO reduction by surface migration of a chemisorbed hydrogen atom [27]. This is also in agreement for Ni–Pd/Alnf, whereby the Ni–Pd alloy reduction peak appears at 345 °C, which is higher than that for Pd/Alnf (110 °C).

The total H_2 consumption for Ni/Alnf was equivalent to only ca. 80% of the theoretical requirement for complete reduction after TPR at 820 °C. However it was in excess of 90% for both Ni–Pt/Alnf and Ni–Pd/Alnf even though the TPR in this case was carried out to only 700 °C. In another result (Fig. 3b), TPO of Ni–Pt/Anf reduced at 500 °C for 5 h with pure H_2 proved that it goes through complete reduction (according to the total oxygen consumption), whereas, TPO of Ni/Alnf after the same reduction process showed that only ca. 60% reduction was achieved. It has been reported that Ni catalyst is not completely reduced on an alumina support due to nickel aluminate ($NiAl_2O_4$) formation during the calcination step of catalyst preparation [26,28,29]. It may be possible that the presence of Pt in the catalyst inhibits the formation of $NiAl_2O_4$ during calcination. Moreover, the oxidation peak of Ni–Pt/Alnf shifted towards higher temperature by 50 °C compared to Ni/Alnf, suggesting that the addition of Pt may provide increased resistance to oxidation during the reaction conditions [30]. A negative peak was also noticed for O_2 uptake in case of Pt/Alnf, which can be explained by the deoxygenation of PtO_2 at temperatures in excess of 550 °C [10]. We note here that H_2 consumption during TPR of Pt/Alnf and Pd/Alnf was also lower than the theoretical requirement (Pt/Alnf = 54%, Pd/Alnf = 28%), but this is because the catalysts go through partial reduction at room temperature, while the reactor cell is purged with H_2/N_2 mixed gas.

3.3. Temperature programmed desorption results

CO–TPD was carried out over all the catalysts listed in Table 1 (illustrated in Fig. 4). The mechanism of desorption is complex and not always well understood [27]. However, it is clear that rate of desorption is largely a function of coverage. The rate is given by following the equation [27]

$$r' = Kf'(\theta)e^{-E'/RT}, \tag{3}$$

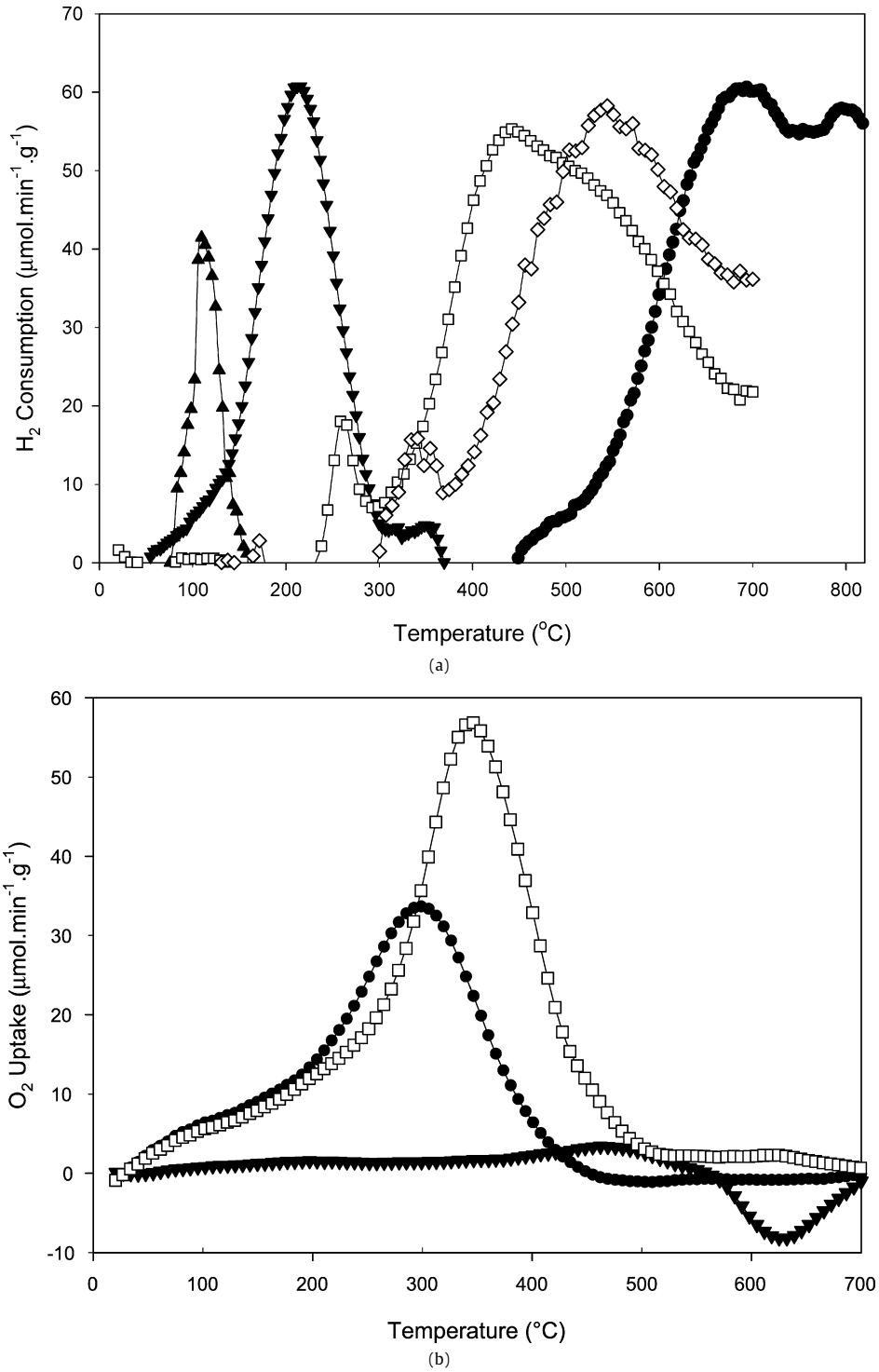

Fig. 3. (a) TPR profiles of the mono- and bimetallic catalysts supported on alumina nano-fibre (Alnf). (b) TPO profiles of Ni and Pt mono- and bimetallic catalyst after normal reduction procedure. Pt/Alnf (▼), Ni/Alnf (●), Pd/Alnf (▲), Ni–Pt/Alnf (□), Ni–Pd/Alnf (◇).

where, K is the rate constant, E' is the activation energy of desorption, and $f'(\theta)$ is the fraction of site available for desorption at coverage θ. E' is related to the heat q and activation energy E of adsorption.

$$E' = q + E, \tag{4}$$

where, E is the activation energy for adsorption.

Therefore it is evident that E' will vary with θ because q is a function of θ. Likewise, K may vary because the frequency of surface bond vibration varies with θ and also because of the heterogeneity of the surface.

It is known from literature [27] (also shown in Section 3.5) that q falls as θ increases. Therefore there will be a significant change in E' and hence the rate of desorption will be very rapid at the low activation energy sites. Keeping this in mind we discuss the results of the rate of CO desorption illustrated in Fig. 4a. Moreover, Fig. 4a must be studied together with Fig. 4b because, in regards to CO desorption over alumina nano-fibre, part of CO is converted to CO_2 which can be a result of the combination of two reactions, namely

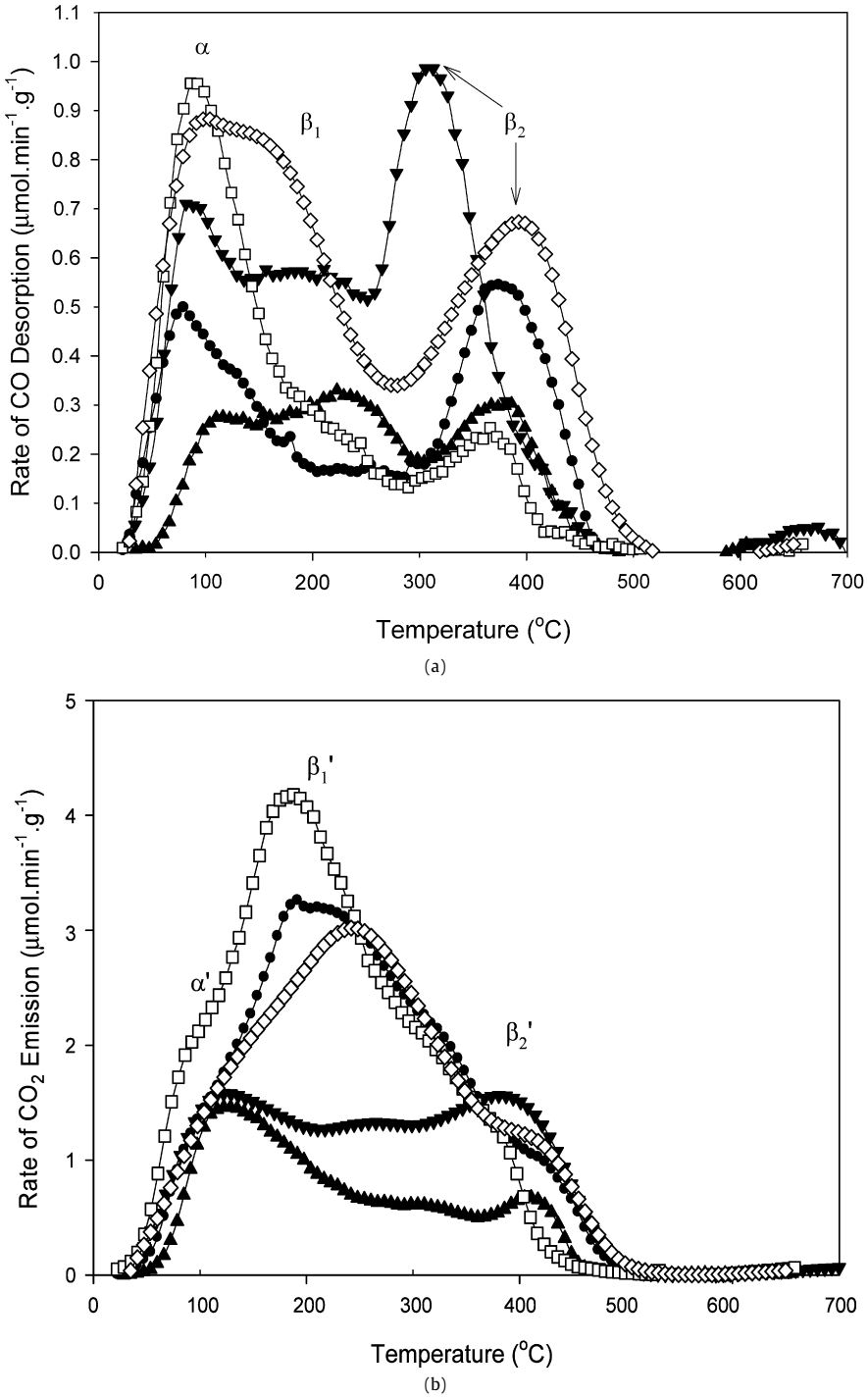

Fig. 4. Results from CO–TPD of monometallic and bimetallic catalysts over alumina nano-fibre support; (a) rate of CO desorption (b) rate of CO_2 emission, produced during CO desorption. Pt/Alnf (▼), Ni/Alnf (●), Pd/Alnf (▲), Ni–Pt/Alnf (□), Ni–Pd/Alnf (◇).

the water gas shift (WGS) and Boudouard reaction, largely dominated by the former reaction. Jackson et al. [31] suggested that the WGS reaction during CO desorption occurs probably because of the dehydroxilation of alumina (Eq. (5)), while, Noronha et al. [32] suggested that in the absence of sufficient OH groups CO goes through the Boudouard reaction (Eq. (6)). These reactions occur because of the high temperatures required for desorption, which cause the adsorbed layer to become largely mobile. As a result, the equilibrium distribution of the adsorbate may interact with each other (Eq. (5)) and with OH groups present on the metal oxide support surface (Eq. (6)). The reactions are as follows

$$2CO \leftrightarrow CO_2 + C, \tag{5}$$

$$2CO + 2OH_{Al_2O_3} \leftrightarrow 2CO_2 + H_2. \tag{6}$$

From Figs. 4a and 4b it is evident that the peaks can be categorised in three broad regions in the rate of CO desorption (α, β_1, β_2) and also in the corresponding rate of CO_2 emission ($\alpha', \beta_1', \beta_2'$) for all the catalysts. Figs. 5a and 5b shows the deconvolution of the overlapping peaks for Ni/Alnf and Ni–Pt/Alnf (others not shown). The fitted curve, which is summation of the Gaussian function peaks, closely represents the raw data. The peaks at low temperature represents desorption of low activation energy (E') sites. Accordingly

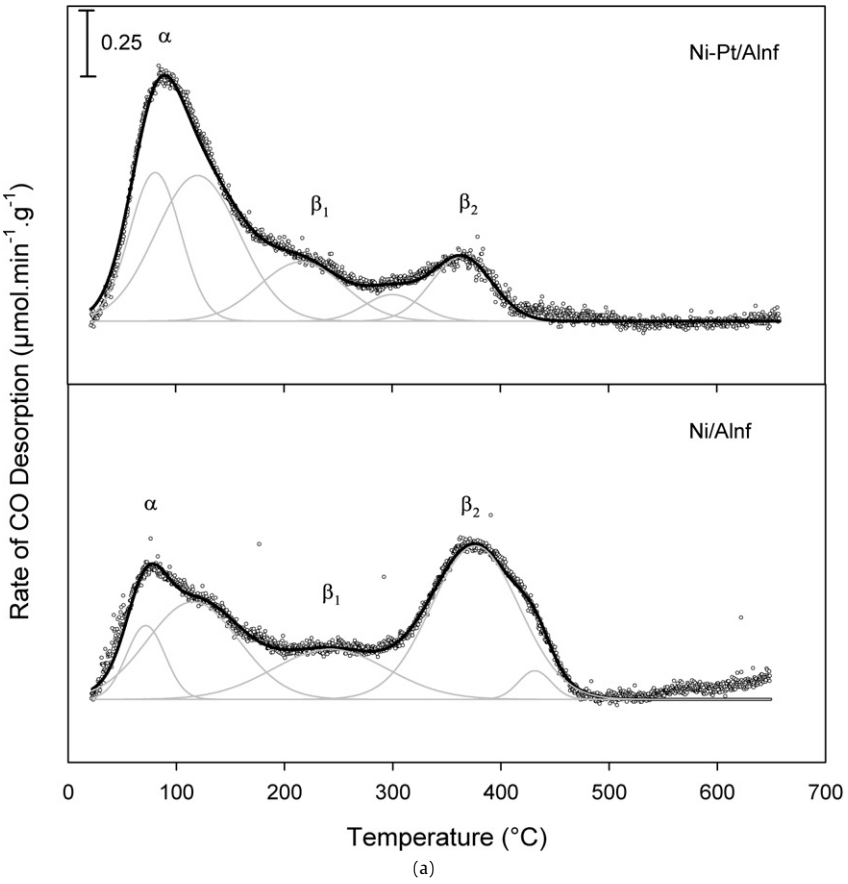

(a)

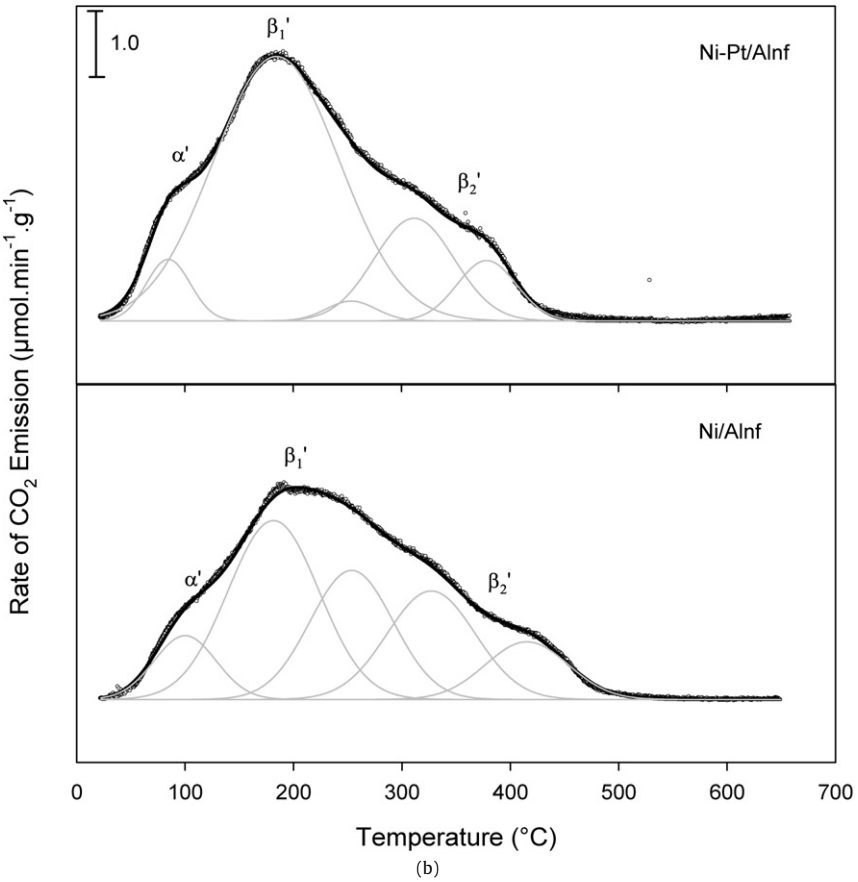

(b)

Fig. 5. Deconvolution of peaks recorded in the results from CO–TPD of Ni/Alnf and Ni–Pt/Alnf catalysts; (a) rate of CO desorption (b) rate of CO_2 emission, produced during CO desorption. The raw data (dotted points) was used in Fityk software version 0.8.6 to generate Gaussian function peaks (grey curves). The sum of the Gaussian function peaks (black curve) were fitted on the raw data using Levenberg–Marquardt method.

these sites have low heat of adsorption (q) or high coverage θ. It can be noted here that the distribution of strength of CO binding sites is most likely to be a continuous probability density function. It is, however, safe to assume in this argument that the Gaussian peaks represent an interval of individual activation energy (E') values [33]. It is believed that the peaks in α region are most likely desorption from a single site chemisorption and the latter two from two site chemisorption [27,34,35]. Hayward et al. [27] suggested that the two site chemisorption is believed to take place at low coverage. At higher coverage the single site chemisorption is dominant. They also reported from literature [36] that mixed one and two site chemisorption was observed on Ni, whereas single site chemisorption dominated on both Pt and Pd. We can also note from the literature [36] that the nature of support plays an active role in determining the two types of adsorption. Pt supported on alumina was reported to exhibit more two site chemisorption compared to silica support. The mechanism of the single and two site chemisorption can be due to heterogeneity [27,36] and adsorption on different lattice spacing [37]. In conclusion we can say that the desorption peaks in Figs. 4 and 5 have different heats of chemisorption in the order $\alpha < \beta_1 < \beta_2$ because of the inverse order of their surface coverage.

The most interesting observation from Figs. 4a and 5a is the increase in peak heights in the α and β_1 regions (and simultaneous decrease in the peak heights in the β_2 region) for bimetallic catalysts when compared to monometallic catalysts. A corresponding change in CO_2 emission can also be noted from Figs. 4b and 5b. Both Ni–Pt/Alnf and Ni–Pd/Alnf show the highest rate of CO-desorption in the α region i.e. low E', suggesting an increase in low heat of adsorption sites—Eq. (4) shows that E' is lowered with decreasing q. The addition of Pt and Pd to the Ni may form surface alloys and create heterogeneity or different lattice spacing leading to decrease in two site chemisorption.

Additionally, the integral of CO and CO_2 desorption peaks i.e. the total CO released (desorbed + converted to CO_2) was found to be in close agreement with the CO chemisorption results in Table 1. For example, the total CO released for Pt/Alnf was 97.40 μmol/gm, for Ni/Alnf it was 92.67 μmol/gm and for Ni–Pt/Alnf it was 102.93 μmol/gm.

3.4. Temperature programmed oxidation results

To illustrate that conversion of CO to CO_2 during CO–TPD was dominated by the WGS reaction, we carried out TPO of the catalysts immediately after the CO–TPD experiment. If the Boudouard reaction took place during the desorption experiment we would expect to see combustion of the carbon deposited on the catalyst as CO_2 emission peak. This CO_2 emission peak could then be integrated to calculate the amount of carbon deposit. In Fig. 6 we only illustrate the TPO analysis carried out over Ni/Alnf, Pt/Alnf and Ni–Pt/Alnf for better clarity of the chart. The solid curves indicate the CO_2 emission from the carbon combustion and the bullet curves represent O_2 uptake during the process. We note here that the O_2 uptake peak does not coincide with the CO_2 emission peak. This is because the O_2 uptake is dominated by the oxidation of the catalysts as evident from the scale of the peak which is 1 to 2 orders of magnitude higher than the CO_2 emission peak. We also notice the negative peak for O_2 uptake in case of Pt/Alnf at temperatures in excess of 550 °C which is similar to the result in Fig. 3b. The CO_2 emission from Pt/Alnf and Ni–Pt/Alnf peaks at 410 and 425 °C respectively, indicating that it was likely to be formed on metal or metal–support interface sites, similar to the results published by Marècot et al. [38]. The CO_2 peak for Ni/Alnf, however, is at 200 °C indicating that it was formed on the metal site [38]. The integral of CO_2 emission peaks suggests that the amount of CO_2 released by the Boudouard reaction during the CO–TPD accounted for only 2.8% for Pt/Alnf and 9.1% for Ni–Pt/Alnf on a molar basis. However, the amount of CO_2 released in TPO of Ni/Alnf was 17.8% of CO_2 released during CO–TPD, suggesting that the Boudouard reaction is more dominant on the Ni catalyst compared to both the Pt and Ni–Pt bimetallic catalysts.

It should be noted here that an organic surfactant was used in synthesising alumina nano-fibre and although it was calcined at 500 °C for 20 h after drying the gel, and for a further 5 h at 500 °C after metal impregnation, any remaining carbon could conceivably be combusted in the TPO runs. Therefore, to test that there was no carbon remaining on the support, TPO was conducted on the alumina nano-fibre support and we could not detect any CO_2 released during the process. Therefore, the remainder of the CO_2 emission is considered to be entirely due to the WGS reaction. WGS reaction is an important step for higher H_2 selectivity production from oxygenated hydrocarbons [3]. Addition of noble metals such as Pt and Pd to the Ni catalyst may suppress the Boudouard reaction, promoting the WGS reaction in the process leading to higher H_2 yield.

3.5. Microcalorimetry results

It was necessary to compare the results obtained from the CO–TPD experiments with direct measurement of heat of adsorption to confirm the findings. Therefore, microcalorimetry experiments were carried out in the heat flux calorimeter using CO as the probe molecule. The differential heat of adsorption (in kJ/mol) was plotted as a function of the adsorbate coverage (in μmol/gm), as shown in Fig. 7. The differential heat profiles are characterised by a plateau of nearly constant heat of adsorption at low coverage (15–20 μmol/gm) followed by an abrupt decrease as the surface saturation limit is reached. In the low coverage plateau region the adsorption of CO can be considered to be strongly bonded and at high coverage the differential heat of CO adsorption represents an average heat from the various adsorption sites on the surface of a given catalyst particle. Therefore, we compare only the initial heat of adsorption when the CO chemisorption may be considered to be equilibrated. The initial heat of CO adsorption on Pd/Alnf was found to be highest (130.09 kJ/mol) followed by Pt/Alnf (122.73 kJ/mol) and Ni/ALnf (116.79 kJ/mol). The initial heat of CO adsorption on Ni–Pt/Alnf was recorded as 111.28 kJ/mol, which is lower than both Pt/Alnf and Ni/Alnf. Similarly, the initial differential heat of Ni–Pd/Alnf (109.60 kJ/mol) was lower than both the corresponding monometallic catalysts. This indicates that the addition of noble metals, even in small fractions, to the Ni catalyst has a significant but weaker promoting effect on the adsorption of CO.

It was suggested earlier that the Pt and Pd forms near surface alloys with Ni and causes changes in the lattice spacing [39]. According to the theoretical calculation of Greeley et al. [40] some of the near surface alloys including Ni/Pt may cause lowering of CO-binding energy leading to a decrease in heat of adsorption. This is an ideal property in a reforming catalyst because it can avoid strong preferential adsorption of CO on the metal, while freeing up that extra fraction of the active sites available for reforming reactions. It has been known for a long time [27] that an ideal catalyst should not have either too strong or too weak adsorption for the reactant. Therefore, by lowering the binding energy of CO over the alloy catalysts it can be expected that the WGS reaction will be favoured during the reforming reaction leading to greater selectivity of H_2 formation.

3.6. TEM, STEM/EDX results

TEM micrographs and EDX analysis of the bimetallic and monometallic catalysts were carried out to visually confirm the

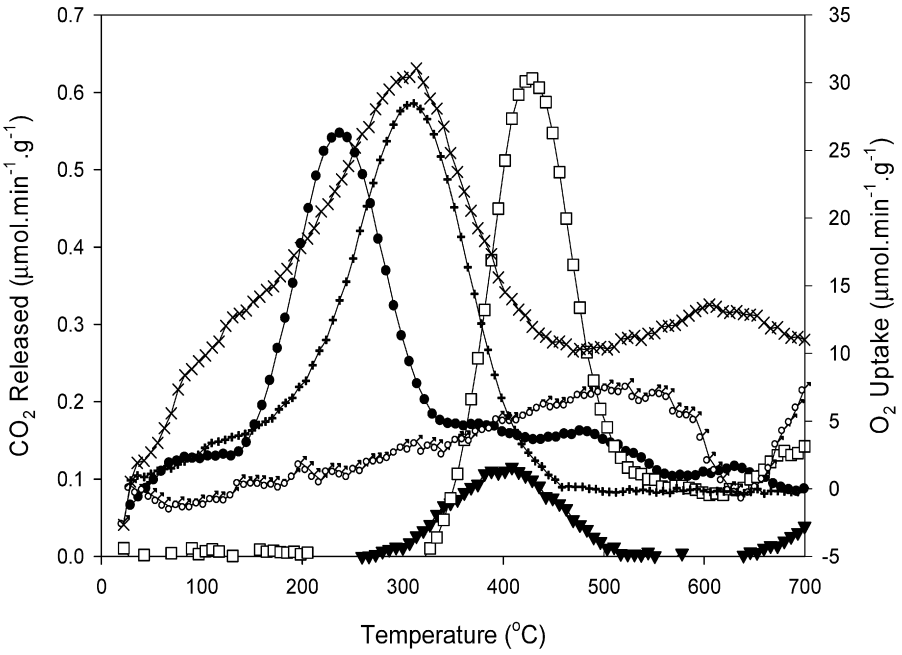

Fig. 6. TPO profile of the alumina nano-fibre supported catalysts after the CO–TPD experiment shows CO_2 released from Pt/Alnf (▼), Ni/Alnf (●) and Ni–Pt/Alnf (□). The O_2 uptake for Pt/Alnf (♂), Ni/Alnf (+) and Ni–Pt/Alnf (×) is shown on the right *Y*-axis. After the CO–TPD run the catalysts were cooled down to room temperature under flowing ultrahigh purity He before starting the TPO run with 2% O_2/He mixed gas.

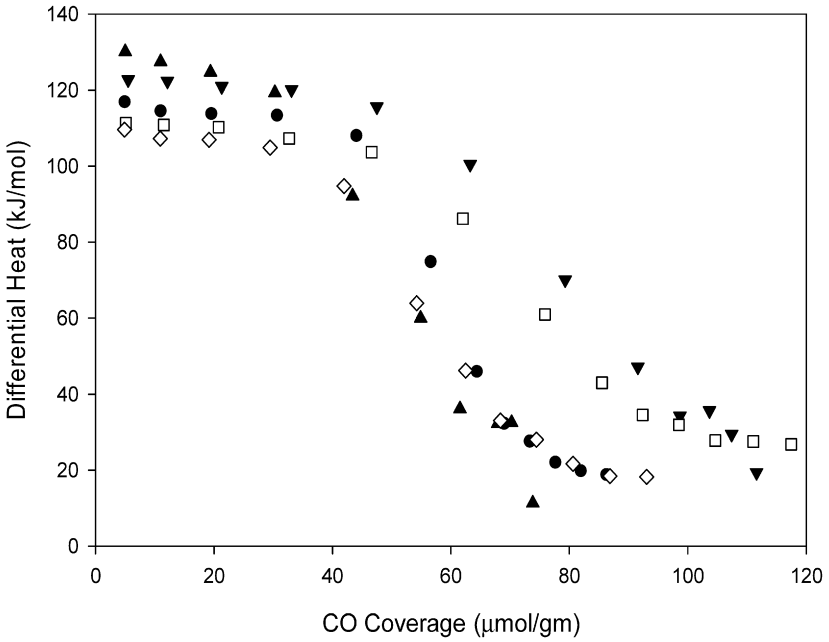

Fig. 7. Results from microcalorimetry of mono- and bimetallic catalysts over alumina nano-fibre. Pt/Alnf (▼), Ni/Alnf (●), Pd/Alnf (▲), Ni–Pt/Alnf (□), Ni–Pd/Alnf (◇).

alloying effect of Pt on Ni. Fig. 8 illustrates the TEM micrographs of Ni/Alnf (a), Ni–Pt/Alnf (b) and the STEM dark field micrograph of Ni–Pt/Alnf (c) and the corresponding EDX spectra (d) of the two points shown on the STEM micrograph. Point 1 was chosen to be on a bulk particle and Point 2 was a single crystal particle. This was chosen because we wanted to observe the distribution of Ni and Pt on the catalyst. The size of the EDX beam was ca. 5 nm.

Initial observation from the TEM micrographs suggests that both the Ni/Alnf and Ni–Pt/Alnf catalysts contain rod shaped particles and are ca. 3 nm across and 10–20 nm in length. However, the Ni/Alnf catalyst largely contains agglomerated particles which are not necessarily rod shaped. All the TEM micrographs taken were of unreduced catalysts, and therefore a decrease in agglomeration can be expected after the catalysts are reduced.

The results from EDX strongly suggest that Ni and Pt emission lines are present in both the bulk and the single crystal particles. The Pt emission lines in a bulk area scan may suggest only the presence of Pt on the support. However, the presence of Pt and Ni emission lines in single-particle EDX spectrum suggests alloy formation. According to the EDX quantification, the atomic concentration of Pt:Ni in the bulk area was 1:33.67 which is in close agreement with the ICP results. The corresponding atomic concentration on the single crystal particle was 1:24. It is believed that Pt and Ni exist as solid solution in mixed oxide form because the cat-

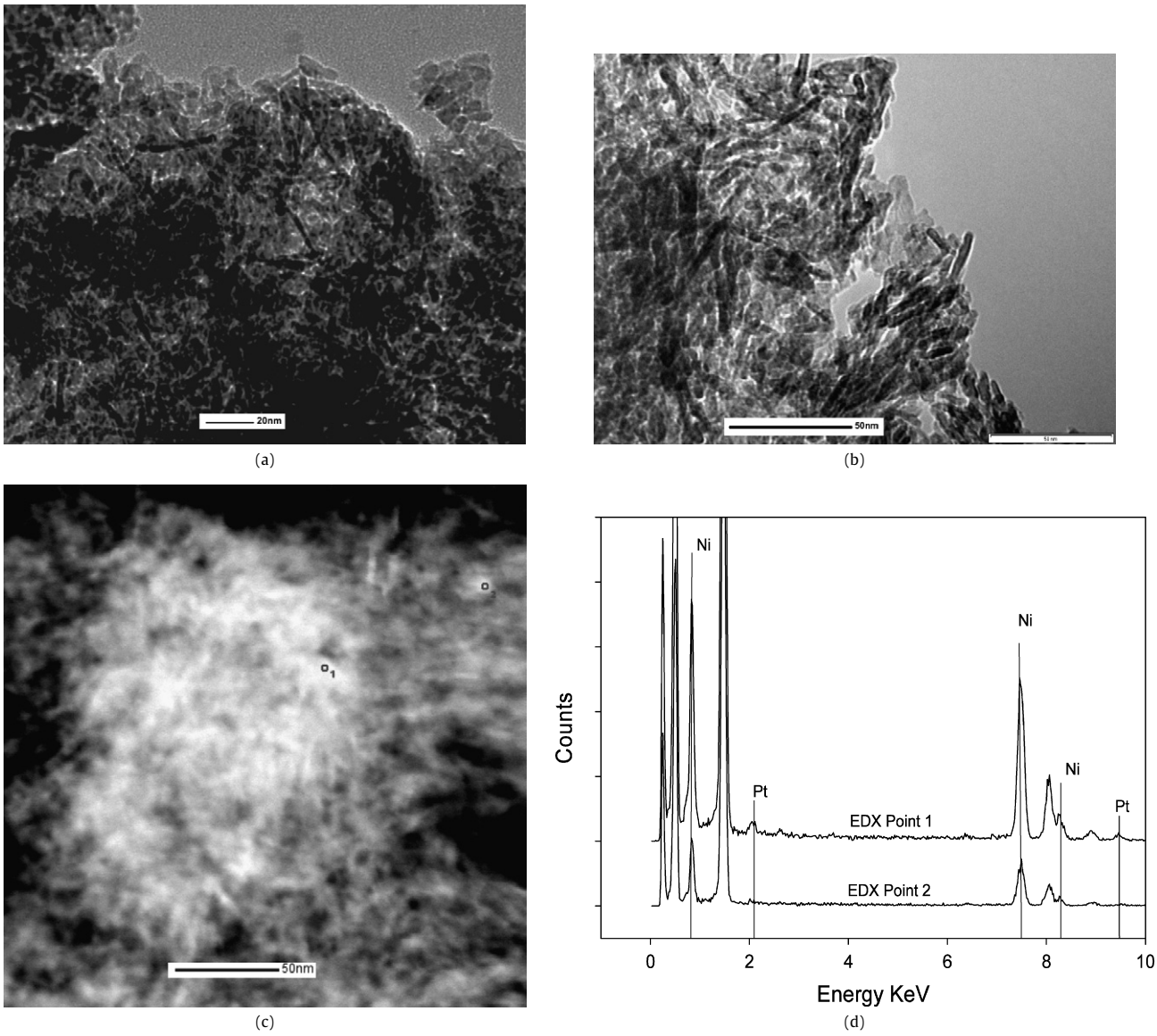

Fig. 8. TEM micrographs of Ni/Alnf (a) and Ni–Pt/Alnf (b); STEM micrograph of Ni–Pt/Alnf (c) and; EDX spectra of point 1 and 2 (d).

alyst was not reduced before EDX. The X-ray count from the single crystal particle was expectedly lower than the bulk particle. Therefore, when represented on the same scale with the bulk particle spectrum, the Pt peaks tend to be difficult to read. However, Pt was indeed detected along with Ni in all the particles we analysed in EDX. Therefore it is most likely that Pt is present in close vicinity of Ni particle, confirming the experimental findings from TPR, TPD and microcalorimetry that Pt and Ni forms an alloy catalyst which results in a decrease in heat of CO adsorption.

3.7. Reaction study of liquid phase reforming of sorbitol

Studies carried out in the fixed bed reactor on mono- and bimetallic catalysts supported on alumina nano-fibre suggests that the addition of Pt and Pd as promoters to Ni, increases its activity to more than three to five times that of Ni/Alnf (Fig. 9a). The rate of H_2 formation increased from 1.5 μmol/min g Cat for Ni/Alnf to nearly 9 μmol/min g Cat for Ni–Pt/Alnf. The gas phase selectivity of the H_2 production shown in Fig. 9a is defined according to the following equation

$$H_2 \text{ selectivity} = \frac{\text{ratio of } H_2/C \text{ in gas phase}}{RR} \times 100, \quad (7)$$

where RR is the reforming ratio for 100% conversion of sorbitol to H_2 and CO_2 according to the following equation [3]

$$C_6O_6H_{14}(l) + 6H_2O \leftrightarrow 13H_2 + 6CO_2. \quad (8)$$

The gas phase selectivity of H_2 production was found to be highest for Pt/Alnf at 79.4% followed by Ni–Pt/Alnf (75.6%) and Ni–Pd/Alnf (66.7%). The selectivity of both Ni/Alnf and Pd/Alnf was less than 50%. The conversion of sorbitol, measured as the change in concentration of sorbitol in water, increased from 35% for Ni/Alnf to 62.5% for Ni–Pt/Alnf (Fig. 9b). We note that the conversion of sorbitol does not equate to the theoretical limit of hydrogen yield (not shown here) because we believe that a considerable fraction of sorbitol does not get converted to a gas phase product. The GCMS results showed presence of propanol, methanol, pentanol and glycolic acid. However, it is evident from Fig. 9b that higher conversion does tend to increase the turn over frequency of H_2 production (TOF in min^{-1} is based of the total CO uptake). These results are in good agreement with the previous studies conducted by Huber et al. [22] where they observed a similar increase in activity of bimetallic catalysts of Pt and Pd for ethylene glycol reforming. We observed a direct correlation between the characterisation studies and the reaction performance of the catalysts.

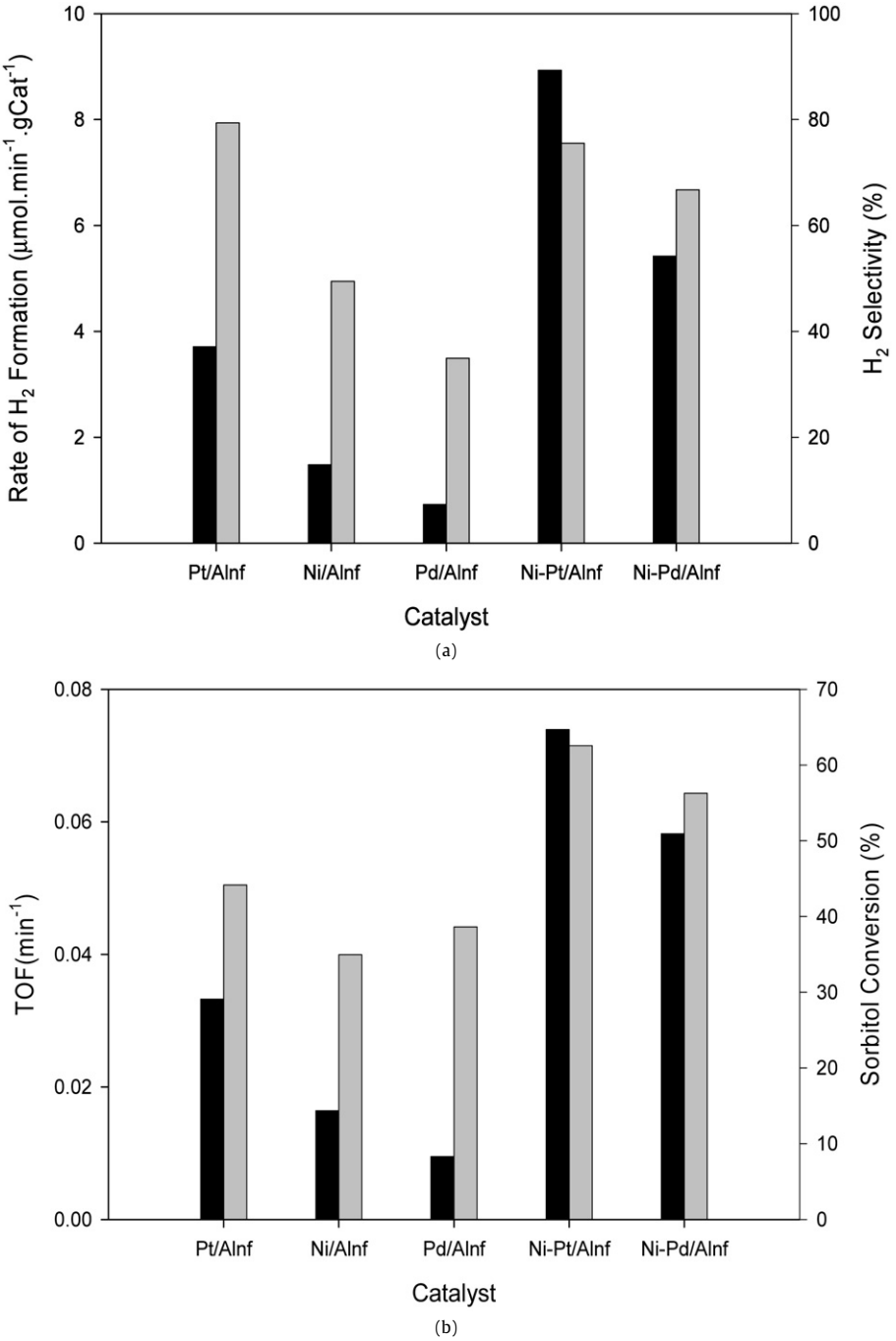

Fig. 9. (a) Rate of H_2 formation (black) and gas phase H_2 selectivity (grey); and (b) TOF based on CO uptake during chemisorption (black) and sorbitol conversion (grey) achieved from the various catalysts supported on Alnf.

4. Conclusion

Temperature programmed reduction was carried out on mono- and bimetallic catalysts of Ni, Pt and Pd. The results, when considered in correlation with chemisorption studies, suggested that the addition of Pt and Pd to Ni catalyst increases the reducibility of Ni catalysts and therefore the number of active sites. Results from temperature programmed desorption suggested that in the case of bimetallic catalysts there was a reduction in the number of strong CO-adsorption sites. It is understood that the alloying effect of these systems leads to the lowering of the CO heat of adsorption. This was confirmed by direct measurement of differential heat of CO chemisorption in the microcalorimetry experiment. We observed that the differential heat of adsorption for Ni–Pt/Alnf reduced to 111.28 kJ/mol, which was 11.45 and 5.51 kJ/mol lower than Pt/Alnf and Ni/Alnf respectively. A similar result was obtained for the Ni–Pd bimetallic catalyst. This was interesting because the atomic ratio of Pt:Ni and Pd:Ni was only 1:33 and 1:18. It was suggested earlier in the literature [39,41] that only a minute amount of surface concentration of solute in the alloy catalysts is sufficient to significantly alter the properties of constituent monometallic catalysts. The TEM and STEM/EDX study was carried out to confirm the presence of Pt in close vicinity of Ni particles in the Ni–Pt/Alnf catalyst. The results provided us the evidence that both Pt and Ni are present in nano-sized rod shaped particles. The reaction study conducted on the fixed bed reactor provided the evidence that the bimetallic catalysts exhibit substantially greater activity than the corresponding pure metal catalysts. The rate of H_2 formation from

Ni–Pt/Alnf was more than five times greater than Ni/Alnf and the sorbitol conversion also increased substantially.

Acknowledgments

The first author acknowledges that a part of the research conducted for this study was undertaken at the Chemical and Biological Engineering Department, University of Wisconsin, Madison, USA, as a recipient of the Graduate Student Research Travel Grant provided by the Graduate School, University of Queensland, Australia. Authors also acknowledge the funding and in-kind support from ARC Centre of Excellence for Functional Nanomaterials.

References

[1] R.R. Davda, J.W. Shabaker, G.W. Huber, R.D. Cortright, J.A. Dumesic, Appl. Catal. B 43 (2003) 13.
[2] J.W. Shabaker, R.R. Davda, G.W. Huber, R.D. Cortright, J.A. Dumesic, J. Catal. 215 (2003) 344.
[3] R.D. Cortright, R.R. Davda, J.A. Dumesic, Nature 418 (2002) 964.
[4] A. Tanksale, Y. Wong, J.N. Beltramini, G.Q. Lu, Int. J. Hydrogen Energy 32 (2007) 717.
[5] A. Tanksale, Y. Wong, J.N. Beltramini, G.Q. Lu, in: C. Jagadish, G.Q.M. Lu (Eds.), Proc. Int. Conf. on Nanoscience and Nanotechnology, Brisbane, 3–7 July 2006, IEEE, p. 540.
[6] B.S. Caglayan, A.K. Avci, Z.I. Oensan, A.E. Aksoylu, Appl. Catal. A 280 (2005) 181.
[7] J.M. Rynkowski, T. Paryjczak, M. Lenik, Appl. Catal. A 126 (1995) 257.
[8] K. Arishtirova, B. Pawelec, R.N. Nikolov, J.L.G. Fierro, S. Damyanova, React. Kinet. Catal. Lett. 91 (2007) 241.
[9] C. Crisafulli, S. Scire, S. Minico, L. Solarino, Appl. Catal. A 225 (2002) 1.
[10] J.M. Rynkowski, T. Paryjczak, M. Lenik, M. Farbotko, J. Goralski, J. Chem. Soc. Faraday Trans. 91 (1995) 3481.
[11] A.F.H. Wielers, M.M.M. Dings, C.J.G. Van der Grift, J.W. Geus, Appl. Catal. 24 (1986) 299.
[12] J.M. Dominguez, E.A. Vazquez, S.A.J. Renouprez, M.J. Yacaman, J. Catal. 75 (1982) 101.
[13] R.T.K. Baker, J.A. Dumesic, J.J. Chludzinski Jr., J. Catal. 101 (1986) 169.
[14] A. Jentys, B.J. McHugh, G.L. Haller, J.A. Lercher, J. Phys. Chem. 96 (1992) 1324.
[15] C. Raab, J.A. Lercher, J.G. Goodwin Jr., J.Z. Shyu, J. Catal. 122 (1990) 406.
[16] C.G. Raab, J.A. Lercher, J. Mol. Catal. 75 (1992) 71.
[17] E.-Y. Ko, E.D. Park, K.W. Seo, H.C. Lee, D. Lee, S. Kim, Catal. Lett. 110 (2006) 275.
[18] Y. Shu, L.E. Murillo, J.P. Bosco, W. Huang, A.I. Frenkel, J.G. Chen, Appl. Catal. A 339 (2008) 169.
[19] N.A. Khan, L.E. Murillo, J.G. Chen, J. Phys. Chem. B 108 (2004) 15748.
[20] H.H. Hwu, J. Eng Jr., J.G. Chen, J. Am. Chem. Soc. 124 (2002) 702.
[21] D. Pope, D.S. Walker, R.L. Moss, J. Catal. 28 (1973) 46.
[22] G.W. Huber, J.W. Shabaker, S.T. Evans, J.A. Dumesic, Appl. Catal. B 62 (2006) 226.
[23] B.E. Spiewak, P. Levin, R.D. Cortright, J.A. Dumesic, J. Phys. Chem. 100 (1996) 17260.
[24] B.E. Spiewak, J. Shen, J.A. Dumesic, J. Phys. Chem. 99 (1995) 17640.
[25] M.A.H. Lanyon, B.M.W. Trapnell, Proc. R. Soc. A 227 (1955) 387.
[26] J.M. Rynkowski, T. Paryjczak, M. Lenik, Appl. Catal. A 106 (1993) 73.
[27] D.O. Hayward, B.M.W. Trapnell, Chemisorption, second ed., Butterworths, London, 1964.
[28] P. Salagre, J.L.G. Fierro, F. Medina, J.E. Sueiras, J. Mol. Catal. A 106 (1996) 125.
[29] P. Turlier, H. Praliaud, P. Moral, G.A. Martin, J.A. Dalmon, Appl. Catal. 19 (1985) 287.
[30] Y. Mukainakano, B. Li, S. Kado, T. Miyazawa, K. Okumura, T. Miyao, S. Naito, K. Kunimori, K. Tomishige, Appl. Catal. A 318 (2007) 252.
[31] S.D. Jackson, B.M. Glanville, J. Willis, G.D. McLellan, G. Webb, R.B. Moyes, S. Simpson, P.B. Wells, R. Whyman, J. Catal. 139 (1993) 207.
[32] F.B. Noronha, M.A.S. Baldanza, R.S. Monteiro, D.A.G. Aranda, A. Ordine, M. Schmal, Appl. Catal. A 210 (2001) 275.
[33] C. Costa, J.M. Lopes, F. Lemos, F.R. Ribeiro, J. Mol. Catal. A 144 (1999) 221.
[34] G. Ehrlich, J. Chem. Phys. 35 (1961) 2165.
[35] P.A. Redhead, Trans. Faraday Soc. 7 (1961) 641.
[36] R.P. Eischens, W.A. Pliskin, Adv. Catal. 10 (1958) 1.
[37] J.S. Rieck, A.T. Bell, J. Catal. 103 (1987) 46.
[38] P. Marecot, A. Akhachane, J. Barbier, Catal. Lett. 36 (1995) 37.
[39] J. Greeley, M. Mavrikakis, Catal. Today 111 (2006) 52.
[40] J. Greeley, M. Mavrikakis, Nature Mater. 3 (2004) 810.
[41] J.A. Rodriguez, D.W. Goodman, Science 257 (1992) 897.